(1)

UNIVERSITY OF SOUTHERN CALIFORNIA

SCHOOL OF ENGINEERING

UNIVERSITY OF SOUTHERN CALIFORNIA

JOINT SERVICES ELECTRONICS PROGRAM
RESEARCH IN ELECTRONICS

F49620-88-C-0067

SECOND ANNUAL TECHNICAL REPORT

For the Period
January 1, 1989 through December 31, 1989

Presented to:

The Air Force Office of Scientific Research
Building 410
Bolling Air Force Base, DC 20332

Presented by:

University of Southern California
Electronic Sciences Laboratory
Los Angeles, California 90089-0483

REPORT DOCUMENTATION PAGE

Form Approved
OMB No. 0704-0188

1. AGENCY USE ONLY (Leave blank)	2. REPORT DATE	3. REPORT TYPE AND DATES COVERED
	5 January 1990	2nd Annual Technical Report, 1/1/89 - 12/31/89

4. TITLE AND SUBTITLE
Joint Services Electronics Program Research in Electronics

5. FUNDING NUMBERS

6. AUTHOR(S)
W. H. Steier, Principal Investigator

7. PERFORMING ORGANIZATION NAME(S) AND ADDRESS(ES)
University of Southern California
University Park
Los Angeles, CA 90089-0483

8. PERFORMING ORGANIZATION REPORT NUMBER

9. SPONSORING/MONITORING AGENCY NAME(S) AND ADDRESS(ES)
AFOSR
Building 410
Bolling AFB, DC 20332

10. SPONSORING/MONITORING AGENCY REPORT NUMBER
F49620-88-C-0067

11. SUPPLEMENTARY NOTES

12a. DISTRIBUTION/AVAILABILITY STATEMENT

12b. DISTRIBUTION CODE

13. ABSTRACT (Maximum 200 words)

This report documents the progress made on the 13 research topics supported by the Joint Services Electronics Program for the period 1/1/80 through 12/31/89. There are four research topics in solid state electronics, four in quantum electronics, and five in information electronics.

14. SUBJECT TERMS
Electronic Materials, Semiconductors, Quantum Electronics, Lasers, Communications, Signal Processing, Computers, Controls

15. NUMBER OF PAGES
52

16. PRICE CODE

17. SECURITY CLASSIFICATION OF REPORT	18. SECURITY CLASSIFICATION OF THIS PAGE	19. SECURITY CLASSIFICATION OF ABSTRACT	20. LIMITATION OF ABSTRACT

UNIVERSITY OF SOUTHERN CALIFORNIA

JOINT SERVICES ELECTRONICS PROGRAM
RESEARCH IN ELECTRONICS

F49620-88-C-0067

SECOND ANNUAL TECHNICAL REPORT

For the Period

January 1, 1989 through December 31, 1989

Presented to:

The Air Force Office of Scientific Research
Building 410
Bolling Air Force Base, DC 20332

Presented by:

University of Southern California
Electronic Sciences Laboratory
Los Angeles, California 90089-0483

TABLE OF CONTENTS

UNIVERSITY OF SOUTHERN CALIFORNIA

Joint Services Electronics Program
Contract No. F49620-88-C-0067

RESEARCH IN ELECTRONICS

Director's Overview

Introduction

This report summarizes the progress made under the Joint Services Electronics Program for the period 1 January 1989 through 31 December 1989. It is the second annual progress report on the 3-year contract, F49620-88-C-0067. The report covers the 13 research projects being supported: four in solid state electronics, four in quantum electronics, and five in information electronics.

Technology Transfer

The transfer of the technology developed under JSEP support into industry in the United States is one of the most important goals of the program. The primary and most effective means of technology transfer is through technical publications and through students who graduate and take, first hand, the developed technology into industrial jobs. The individual research units give reference to 35 publications which appeared in print or were accepted for publication in 1989, and which directly resulted from JSEP support during this past year. Numerous other publications were submitted to journals during the year. These publications have been published or presented in a wide scope of technical forums and the scientific results achieved have, therefore, been widely disseminated.

Four Ph.D. theses have been completed during this past year which are directly due to JSEP support. The continuity of JSEP support has been one of hte major factors in the continued high productivity of the faculty, both in publications and in the number of students graduated.

Selective Area Epitaxial Growth of Photonic Structures by Metalorganic Chemical Vapor Deposition

P. Daniel Dapkus

Research Unit SS2-1

Progress

In last year's report, we described investigations of the low temperature (<425°C) growth of GaAs by thermally-driven atomic layer epitaxy (ALE). This was undertaken to develop a better understanding of the laser assisted ALE process which shows a marked increase in growth rate only in this temperature regime. These studies showed that the surface reaction rate of TMGa was quite slow below 400°C requiring ~10 sec of TMGa exposure at 400°C to complete one monolayer of GaAs after AsH_3 exposure. For shorter times, less than one monolayer was formed suggesting that the initial adsorbates were partially decomposed or undecomposed TMGa that hindered the absorption of the gallium species on nearby sites owing to their large physical size.

By contrast, in work performed over one year ago, we showed that the time to form a monolayer of GaAs in photoassisted ALE can be as short as 10 msec at these temperatures. This result suggests that the steric hindrance is minimized under photoexcitation, presumably because of the enhanced surface reaction rates induced by the photoexcitation. To provide a more complete understanding of these effects and to provide a better description of the role of photostimulated and photothermal processes in laser assisted ALE, we have undertaken both fundamental and empirical studies of the laser ALE process. The fundamental studies, which are partially supported by ONR, are directed at measuring the rates of surface reactions under thermal and laser driven conditions. The empirical studies are directed at developing a more complete understanding of the parametric dependence of the laser ALE growth rate and materials properties.

Laser ALE Growth Mechanism Study

Our initial experiments have focussed in a study of the saturation mechanisms responsible for thermally driven ALE. In these studies, we have utilized the UHV

XPS/reaction chamber system that was developed with URIP support and made operational with ONR support. The system consists of a UHV deposition chamber with a TMGa and an As_4 source coupled to a PHI 5100 XPS system that contains a RHEED gun and phosphor screen. The combination of XPS and RHEED permits us to identify both the chemical nature of the adsorbed species as well as the resultant surface structure. Experiments were conducted to determine the reaction mechanisms and rates involved in the adsorption of TMGa on As-stabilized 2 x 4 surfaces. For this program, particular emphasis was placed on the temperature range below 400°C where significant photoenhanced ALE is observed under atmospheric pressure conditions. At higher temperature, TMGa was observed to convert an As-stabilized 2 x 4 surface to a Ga-stabilized 4 x X (X = 1, 2) surface with no evidence of carbon or methyl radicals on the surface. The rate of this reaction was observed to be strongly dependent on temperature decreasing with decreasing temperature. Studies are underway under ONR support to measure these rates and the detailed mechanism.

In the temperature range from 320°C to 370°C, no Ga adsorption on the As-stabilized surface was observed for exposures in excess of 200 Langmuirs. We conclude that the adsorption and decomposition reaction rates are significantly smaller than the desorption rates at these temperatures, i.e. TMGa does not "stick". We further suggest that the mechanism responsible for laser assisted ALE at atmospheric pressure involves the local enhancement of the adsorption and decomposition reaction rates caused by the photoexcitation. Specific studies are underway to determine if the photoexcitation results in a change in the surface structure prior to adsorption that enhances this reaction or if the photoexcitation causes a direct enhancement of the surface reaction rate by altering the surface chemistry in some other way.

Empirical Studies of Laser Assisted ALE Growth

In previous work, we were able to selectively deposit GaAs by laser assisted ALE in 30 μm wide stripes by scanning a substrate past a focused laser during TMGa exposure. These small deposits were difficult to characterize. With the recent installation of a 20W argon laser, we are now able to explore growth in stripes as wide as 600 μm. As a result, we have explored the growth of GaAs by laser ALE

under a variety of growth conditions by varying growth temperature, laser power, spot size, and scan speed. We have been able to grow single crystal GaAs at a growth rate of 1 ML/cycle over a wide range of TMGa exposure and laser power, and with scan rates that range from 3 mm/sec to 10 mm/sec. The deposits show a flat top deposit characteristic of ALE growth (see Fig. 1). We are currently studying the dependence of materials properties on the growth parameters previously described, as well as AsH_3 exposure time, concentration, and temperature. As the materials properties improve, we will incorporate these materials into device structures for device evaluation.

FIGURE 1. Surface Profilometer Plot of GaAs Deposit Grown by Laser Assisted ALE at 400°C. The profile shows marked flattening of the top of the deposit because of ALE saturated growth.

Publications

1. P. D. Dapkus, S. P. DenBaars, Q. Chen, W. G. Jeong, and B. Y. Maa, "The Role of Surface and Gas Phase Reactions in Atomic Layer Epitaxy," Prog. Crystal Growth and Charact. **19**, 137 (1989).

2. W. G. Jeong, E. P. Menu, and P. D. Dapkus, "Atomic Layer Epitaxy of GaAs and InAs," Mat. Res. Soc. Symp. Proc., **145**, 163 (1989).

3. R. Singh and L. J. Messick, "Indium Phosphide and Related Materials for Advanced Electronic and Optical Devices," Proceedings Reprint, 1st Intl. Conf., **SPIE 1144**, Norman, OK (March 1989).

4. B. Y. Maa and P. D. Dapkus, "RHEED and XPS Observations of Trimethylgallium Adsorption on GaAs (001) Surfaces -- Relevance to Atomic Layer Epitaxy," to be published in J. Electronic Materials (1990).

Strain Induced Metastability in Heterostructures: Some Investigations of Molecular Beam Epitaxial Growth and Interconversion of Metastable States

Anupam Madhukar **Research Unit SS2-2**

Progress

During this reporting period (January through December 1989), work was continued on two parallel thrusts: (1) development of a focused ion beam (FIB) system for investigations of the ablation (i.e., direct write) characteristics of metastable III-V strained layers and strained fluoride films, (2) growth, fabrication, and testing of strained GaAs/InGaAs/AlAs system based resonant tunnelling diodes (RTDs). A brief description of the progress made on these follows:

1. Focussed Ion Beam System for Direct Write Patterning

In the progress report for the previous year, we noted that a custom FIB system capable of being interfaced with the MBE growth system and a PECVD system was designed and placed on order. The anticipated delivery time for the system was Summer 1989. In the course of fabrication of this custom designed system involving four different vendors, certain aspects had to be re-evaluated to, in part, account for advances in individual components as well as additional desired features. A particular improvement though desirable was additional vibration isolation features. This led to a redesign of the FIB ultra-high vacuum chamber and its support system to allow accommodating a vibrationally isolated optical table as the base. A final design of the FIB chamber was agreed upon between RIBER and us (with inputs from FEI and Thermionic Laboratory Inc., the manufacturers, respectively, of the FIB gun and the sample [x,y,z] stage) by October 1989 and is to be delivered in Spring 1990. The FIB gun, supplies, manipulator, (x,y,z) stage, pumping system for the FIB chamber, etc., have all been now delivered.

In parallel, work was undertaken for computer interfacing of the FIB system to write desired patterns. Progress has been made on both hardware and software development. We expect this system to be ready in time for the arrival of the FIB

chamber. With the final assembly of this system in Spring 1990, we shall be enabled to begin examination of the direct write characteristics of strained III-V semiconductor films and of group IIA fluorides deposited on Si, GaAs and InP.

2. Strained GaAs/InGaAs/AlAs Resonant Tunneling Diodes

While awaiting the establishment of the in-situ FIB system for all UHV processing, we undertook examination of the metastable strained InGaAs on GaAs films grown via MBE in the form of resonant tunnelling structures. The central physical concept being exploited here is the notion, developed under separate contracts from ONR for computer simulations and from AFOSR for MBE growth, that growth of strained films on pre-patterned substrates should dramatically reduce the deleterious defect density through strain release at mesa edges. The basic idea having been substantiated through our work sponsored by ONR and AFOSR, we exploited its potential application through growth, fabrication, and testing of GaAs/$In_xGa_{1-x}As$/AlAs system based resonant tunnelling diodes grown on patterned and non-patterned GaAs(100) substrates.

Substantial progress has been made on this front and we have demonstrated the best strained GaAs/$In_xGa_{1-x}As$/AlAs ($x < 0.25$) RTDs to date. As an example, Fig. 1 shows the room temperature I-V characteristics of a typical RTD ($x = 0.25$). A peak-to-valley ratio (PVR) of 4.2 with a peak current (J_p) of 10 KV/Cm^2 is found. The asymmetry in the I-V characteristics of this structure is due to the intentional choice of different thicknesses of the AlAs barrier layers confining the $In_{0.25}Ga_{0.75}As$ well layer. At liquid nitrogen temperature the PVR is 15 and J_p ~12 KA/Cm^2. Details of these and other RTDs are to appear in two publications (see below). Work is continuing on extending the investigations towards higher In content to achieve high room temperature PVR (>10) and high J_p (~10^5 A/Cm^2) needed for practical RTDs.

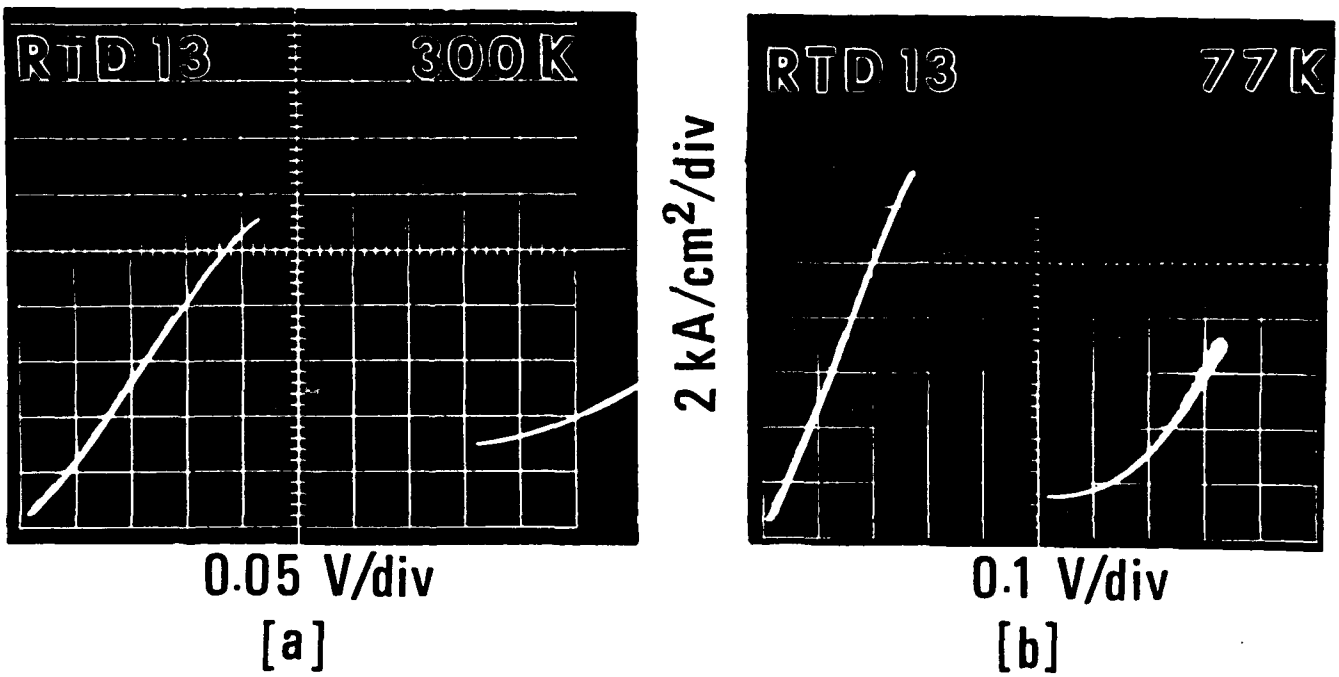

FIGURE 1

Publications

1. R. Kapre, A. Madhukar, K. Kaviani, S. Guha, and K. C. Rajkumar, "Realization and Analysis of GaAs/AlAs/$In_{0.1}Ga_{0.9}As$ Based Resonant Tunneling Diodes with High Peak to Valley Ratios at Room Temperature," App. Phys. Lett (in press).

2. R. Kapre, A. Madhukar, and S. Guha, "$In_{0.25}Ga_{0.75}As$/AlAs Based Resonant Tunneling Diodes Grown on Pre-Patterned and Non-Patterned GaAs(100) Substrates, IEEE Electron Device Letts. (submitted).

3. D. J. Kim, A. Madhukar, W. Chen, K. Z. Hu, "Realization of High Mobilities at Ultra Low Electron Density in GaAs-$A1_{0.3}Ga_{0.7}As$ Inverted Heterojunctions," App. Phys. Lett. (submitted).

ELECTROOPTIC DEVICES FOR OPTICAL INFORMATION PROCESSING AND COMPUTING APPLICATIONS

Armand R. Tanguay, Jr.

Research Unit SS2-3

Progress

During this contract period, the primary focus of the research effort has been on further understanding of the fundamental physical processes that characterize the Photorefractive Incoherent-to-Coherent Optical Converter (PICOC) [JSEP Publ. 1], as well as on the optimization of device performance characteristics. The PICOC device is a two-dimensional spatial light modulator that combines photorefractive volume holographic storage principles with erasure by an incoherent image-bearing light source to effect a high resolution incoherent-to-coherent conversion. This particular approach to the development of a viable spatial light modulation technology has been shown to be characterized by relatively high performance, and at the same time is extremely simple in design and hence capable of inexpensive fabrication in a production environment.

A number of key technical issues are under continuing investigation in parallel, including an extensive investigation of PICOC device performance in conjunction with both photoconductive charge transport and diffractive readout models [JSEP Publs. 1, 2], the discovery and analysis of significant electric field variations within the bulk photorefractive crystal during photorefractive grating formation [JSEP Publ. 3, 4] with their concomitant impact on the temporal response of the diffraction efficiency, an examination of the polarization properties of diffraction from bismuth silicon oxide under conditions of enhanced self-diffraction [JSEP Publ. 2] (which can be employed to optimize the signal-to-noise ratio of the conversion process), the development of an antireflection coating for the PICOC device fabricated from bismuth silicon oxide that is at once characterized by exceptionally low reflection coefficients and a very wide bandpass (both in wavelength and in angle of incidence) [JSEP Publs. 5, 6], an analysis and experimental implementation of the PICOC device constructed with a Stratified Volume Holographic Optical Element (SVHOE) [JSEP Publ. 7], an examination of the fundamental and technological limitations of photorefractive grating formation as they impact current

and projected PICOC device sensitivity [JSEP Publ. 8], and the development of an electrooptic technique for the measurement of the extremely high dark resistivities of as-grown photorefractive crystals [JSEP Publ. 9] (which is important for the incorporation of empirically determined parameters in theoretical models of device performance, for optimization of the crystal growth of photorefractive materials, and for the determination of the stored photorefractive grating decay time constant).

Of the many results that have accrued to the investigation during the past year (as described in the attached publications), perhaps one of the most surprising is the observation of a significant increase in the diffraction efficiency of a photorefractive grating with the incorporation of antireflection coatings on the two opposing surfaces of the photorefractive crystal. This result, described in more detail below, will impact not only the functional performance of PICOC devices that are the primary focus of this investigation.

In these experiments, we designed a two layer antireflection coating for single crystal bismuth silicon oxide ($Bi_{12}SiO_{20}$), which has a relatively high refractive index (2.61) at the grating recording wavelength (typically 514.5 nm). The coating was designed to satisfy a number of conflicting requirements for satisfactory PICOC device operation, including broad wavelength bandwidth (to allow independent choice of grating recording, image recording, and readout wavelengths), very low residual reflectivity at the design wavelength, and broad angular response (since the grating recording beams and the readout beam enter the crystal at highly oblique angles, whereas the image recording beam is incident at near normal incidence). The chosen materials for the two layer coating consisted of magnesium flouride (MgF_2) and zirconium dioxide (ZrO_2), which were evaporated by electron beam techniques from a base pressure of 10^{-8} Torr in a Balzers BAK-640 multisource production box coater.

The results of the coating process are as shown in Fig. 1, in which the wavelength dispersion of the coating design is plotted along with a series of experimental data points, obtained with a number of different laser sources over the wavelength range of interest. As can be seen from the figure, the first two design requirements have been satisfied, and independent measurement of the angular response characteristics showed excellent agreement as well.

Measurements of the diffraction efficiency from a grating recorded in the diffusion regime were made on the same crystal both before and after AR coating, as shown in Fig. 2. In this figure, h_1 is the diffraction efficiency normalized to the incident beam intensity, while h_2 is the diffraction efficiency normalized to the transmitted beam intensity. The diffraction efficiency in both cases is seen to be increased by approximately 100% by means of the incorporation of the AR coating. Of course, it should be expected that the elimination of the first surface reflectivities (approximately 20% per surface) should increase the diffraction efficiency somewhat. What is in fact surprising is that the increase is considerably larger than can be explained by the elimination of the first surface reflectivities alone. A preliminary analysis of the discrepancy shows that the major contribution to the increased diffraction efficiency in fact arises from the elimination of auxiliary diffraction gratings formed among the incident beams transmitted through the first surface, and the retroreflected beams originating at the second surface. These gratings can in fact be comparable in grating modulation to that of the primary grating, depending on the modulation depth of the initially incident beams.

It is important to note that these results are of significance to the development of photorefractive incoherent-to-coherent converters as spatial light modulators for at least two reasons. First, the antireflection coating eliminates spurious reflections in the imaging beam which can significantly compromise image fidelity and spatial resolution. Second, the resultant increase in diffraction efficiency represents a 100% improvement in device recording sensitivity for both the grating recording beams as well as for the image recoding beam.

A second major component of the research program involves the development of silicon-based driver chips for analog (as opposed to the traditional digital) Total Internal Reflection (TIR) Spatial Light Modulators, which have a wide range of applications in optical information processing and computing as discussed in the proposal. During the most recent contract period, considerable progress has been achieved in the design and development of the requisite analog driver circuitry based on the design constraints of the primarily digital Metal Oxide Semiconductor Implementation Service (MOSIS). Our first chip design (developed in parallel for neural network applications as well) has been satisfactorily fabricated in a dual rail configuration that demonstrates dual channel linear performance over the design

input voltage range [JSEP Publs. 10, 11]. The next step is to incorporate high voltage (25 - 50 V) drive transistors that are compatible with the requirements of the load imposed by a proximity coupled electrooptic crystal, in order that fully functional TIR modulators can be fabricated and evaluated.

Publications

1. J. Yu, D. Psaltis, A. Marrakchi, A. R. Tanguay, Jr., and R. V. Johnson, "Photorefractive Incoherent-to-Coherent Optical Conversion", in Photorefractive Materials and Applications, J. P. Huignard and P. Gunter, Eds., Springer-Verlag, New York (1989).

2. A. Marrakchi, R. V. Johnson, and A. R. Tanguay, Jr., "Polarization Properties of Enhanced Self-Diffraction in Sillenite Crystals", IEEE J. Quant. Electron., QE-23, 2142-2151 (1987).

3. E. J. Herbulock, R. V. Johnson, and A. R. Tanguay, Jr., "Electric Field Profile Effects on Photorefractive Grating Formation in Bismuth Silicon Oxide", 1988 Annual Meeting of the Optical Society of America, Santa Clara, California (1988).

4. A. R. Tanguay, Jr., "Device Development for Optical Computing", Conference on Lasers and Electro-Optics (CLEO '89), Baltimore, Maryland (1989); (Invited Paper).

5. Z. Karim, M. H. Garrett, and A. R. Tanguay, Jr., "A Bandpass AR Coating Design for Bismuth Silicon Oxide", 1988 Annual Meeting of the Optical Society of America, Santa Clara, California (1988).

6. Z. Karim, C. Kyriakakis, and A. R. Tanguay, Jr., "Improved Two Beam Coupling Gain and Diffraction Efficiency in Bismuth Silicon Oxide Crystal Using a Bandpass AR Coating", 1989 Annual Meeting of the Optical Society of America, Orlando, Florida (1989).

7. R. V. Johnson and A. R. Tanguay, Jr., "Stratified Volume Holographic Optical Elements", Opt. Lett., 13(3), 189-191 (1988).

8. R. V. Johnson and A. R. Tanguay, Jr., "Fundamental Physical Limitations of the Photorefractive Grating Recording Sensitivity", in Optical Processing and Computing, H. Arsenault and T. Szoplik, Eds., Academic Press, New York (1989).

9. D. A. Seery, M. H. Garrett, and A. R. Tanguay, Jr., "Electrooptic Measurement of the Volume Resistivity of Bismuth Silicon Oxide ($Bi_{12}SiO_{20}$)", J. Cryst. Growth, 85, 282-289 (1987).

10. B. K. Jenkins, G. C. Petrisor, S. Piazzolla, P. Asthana, and A. R. Tanguay, Jr., "Photonic Architecture for Neural Nets Using Incoherent/Coherent Holographic Interconnections", Proc. Intl. Conf. Opt. Comp. (OC '90), Kobe, Japan (1990).

11. P. Asthana, H. Chin, G. Nordin, A. R. Tanguay, Jr., S. Piazzolla, B. K. Jenkins, and A. Madhukar, "Photonic Components for Neural Net Implementations Using Incoherent/Coherent Holographic Interconnections", Proc. Intl. Conf. Opt. Comp. (OC '90), Kobe, Japan (1990).

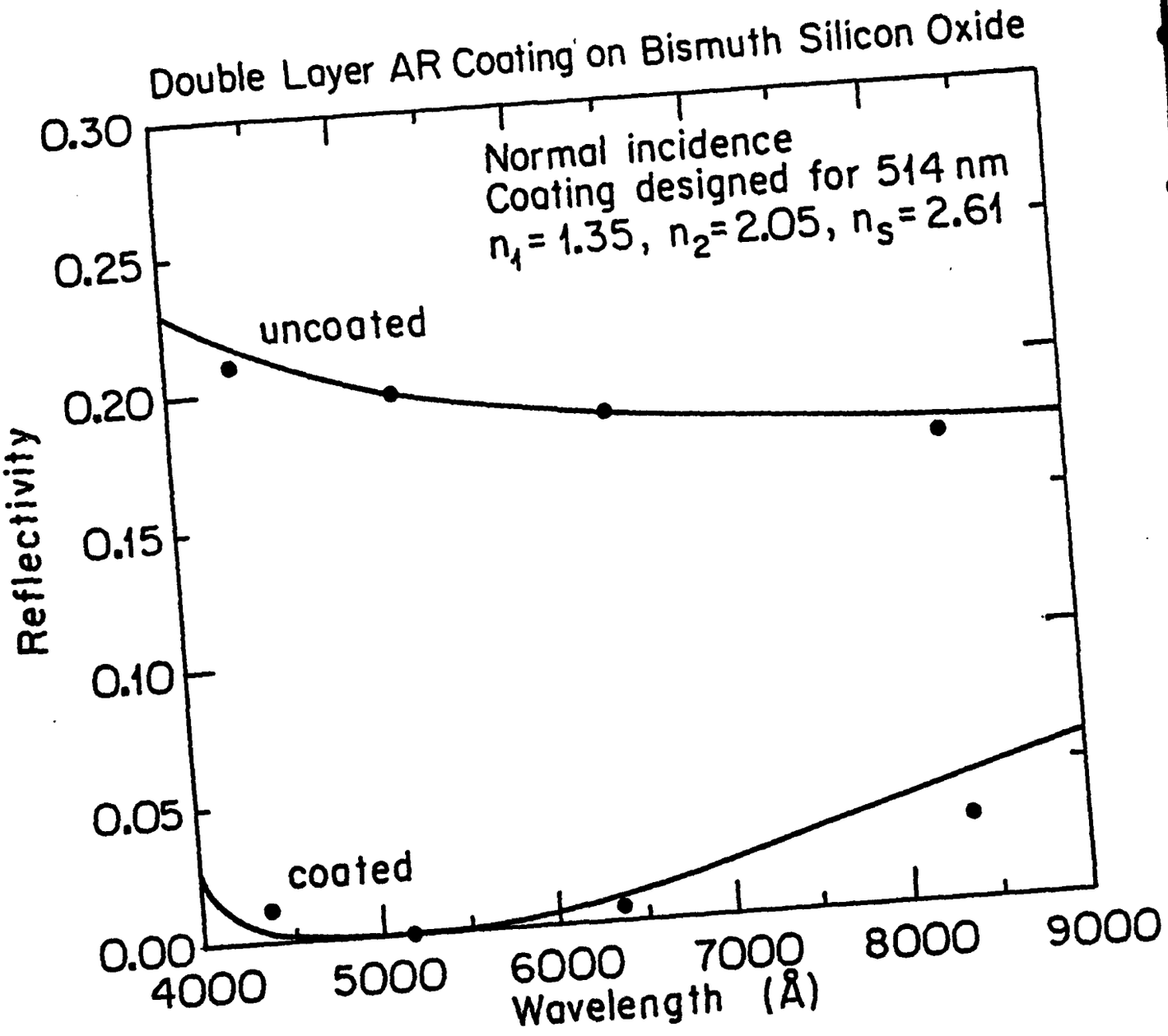

Figure 1. Wavelength dispersion of a MgF_2/ZrO_2 double layer antireflection coating on bismuth silicon oxide, for the case of normal incidence. In this case, the coating was designed for a minimum at 514.5 nm. The design curves are shown solid, while the experimental points were derived from reflectivity measurements made with a variety of laser sources.

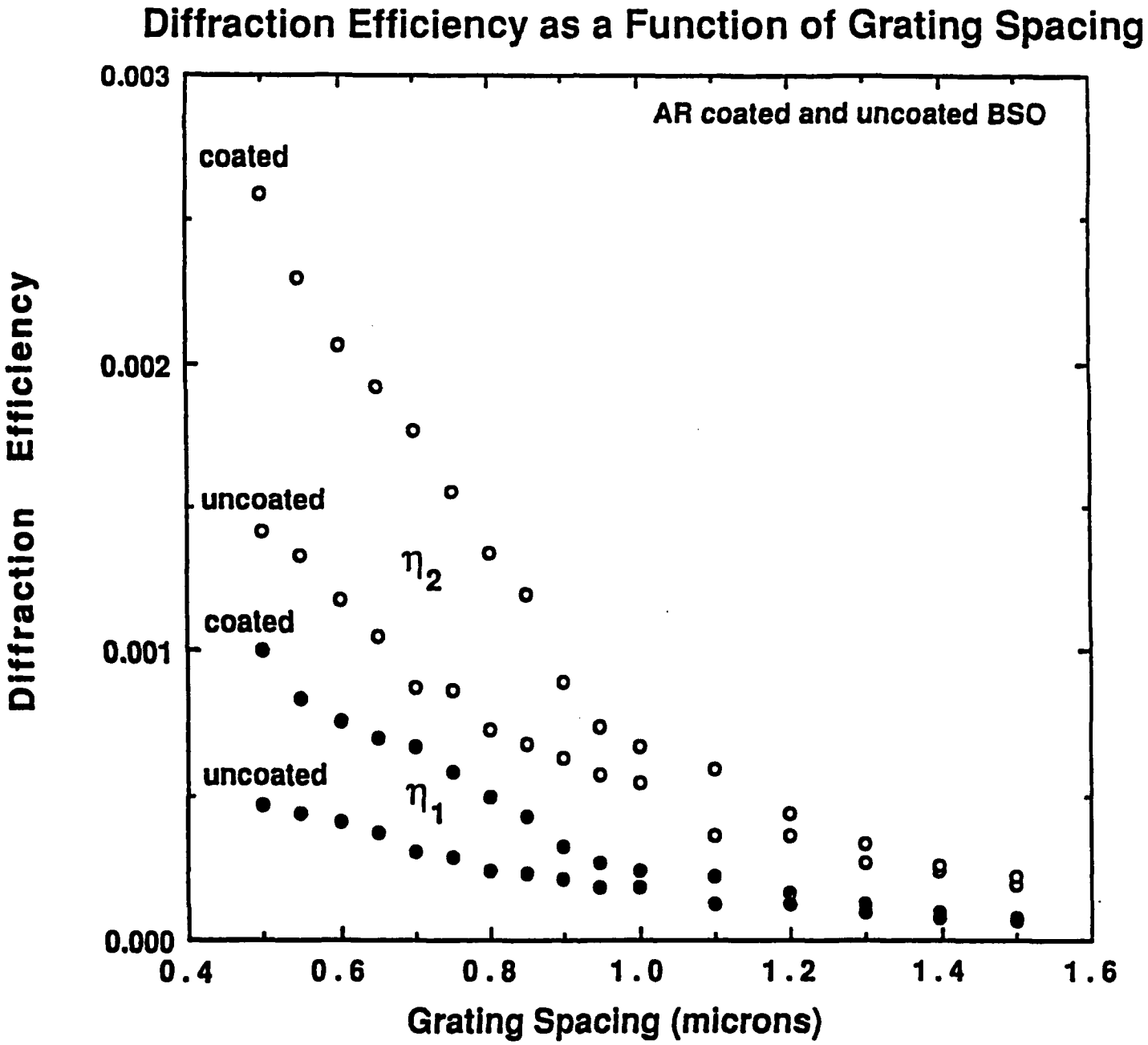

Figure 2. Diffraction efficiency as a function of photorefractive grating spacing for both antireflection coated and uncoated bismuth silicon oxide, showing diffraction efficiencies normalized both to the incident beam intensity (1) and to the transmitted (zero order) beam intensity (2).

Optoelectronic and Quantum Structures Using Pristine and Irradiated Organic Compounds

Stephen R. Forrest

Unit SS2-4

Progress

During this second year of work, we have continued our investigations of the transport of charge across isotype organic heterojunctions. Very high quality heterojunctions which we find are nearly defect free have been grown in a unique, UHV organic molecular beam epitaxy (OMBE) system. By deposition of the organic material onto substrates cooled to 80K, we have shown that highly flat, uniform films down to 10 Å thick have been grown. Further, the films have been demonstrated to be single crystalline across large substrate areas (e.g. 4 cm^2). Using this sophisticated growth technology, on separate funding we have demonstrated, for the first time, the growth of crystalline organic multiple quantum well structures (CO-MQWS) which exhibit single crystallinity even though the two crystalline compounds used to form the alternating layer stacks in the CO-MQW are incommensurate. Also, the structures exhibited exciton confinement within various material layers, and hence should have applications as optoelectronic modulators and detectors in the near future.

The JSEP-funded investigations have benefitted from the single crystalline growth of multilayer structures, since we have studied the optical and charge transport properties across several CO heterojunction (CO-HJ) material pairs. In particular, we have investigated the properties of three heterojunctions consisting of pairs of the following organic semiconductor compounds: 3,4,9,10 perylenetetracarboxylic dianhydride (PTCDA); 3,4,9,10 perylenetetracarboxylic bis benzimidazole (PTCBI); and copper phthalocyanine (CuPc). Here, PTCDA and CuPc were obtained from commercial sources and purified in our laboratory, and PTCBI was synthesized from a combination of PTCDA and o-phenylenediamine, and was then purified in our laboratory.

Deposition of the materials pairs formed two-layer heterojunction devices with good rectifying characteristics suggesting that they form a trio of p-P heterojunctions.

X-ray analysis shows that the resulting HJ's are crystalline, with the stacking habits of the individual components of the HJ similar to their bulk stacking habits. A typical room temperature, current-voltage (I-V) characteristic of a PTCDA/CuPc CO-HJ is shown in Fig. 1.

By analysis of the I-V and capacitance voltage characteristics of the HJ samples, we were able to obtain a measurement of the valence band offset energies (DE_V) at the contacts. We obtained the result that the three HJ pairs (i.e. CuPc/PTCDA, CuPc/PTCBI and PTCDA/PTCBI) follow a transitive relationship, viz:

$$DE_{VA,C} = DE_{VA,B} - DE_{VB,C}$$

Here, the three materials are indexed as material A, B and C. The above relationship suggests that the organic heterojunction offset energies are largely the result of the intrinsic properties of the contacting materials, rather than being influenced by defect charge. If defect charge were a significant contributor to the measured value of DE_V for one or more of the material pairs, large discrepancies to this equation would ensue.

Having determined the band offset energies, it is important to try to understand their interpretation in a system of materials (i.e. organic semiconductors) where the processes of band and hopping conductivity compete due to the localized nature of the charge. That is, the band picture does not completely describe charge transport in such materials, and hence the valence band offset energy as defined above is not necessarily a good description of the properties of such heterojunctions. To this end, we can consider DE_V to be the activation energy for hole transport from one material to the next. In Fig. 2 is shown the CO vibronic energy level diagram as a function of the configuration coordinate, Q, for a CuPc/PTCDA HJ. Here, it can be seen that DE_V is interpreted as the energy difference between the ground states in the HOMO bands in the two contacting materials, and is thus the energy required to transfer a hole across this interface. We also show the existence of a high density of defects at a mean energy of E_T within the energy gap of CuPc. No such level is observed for PTCDA.

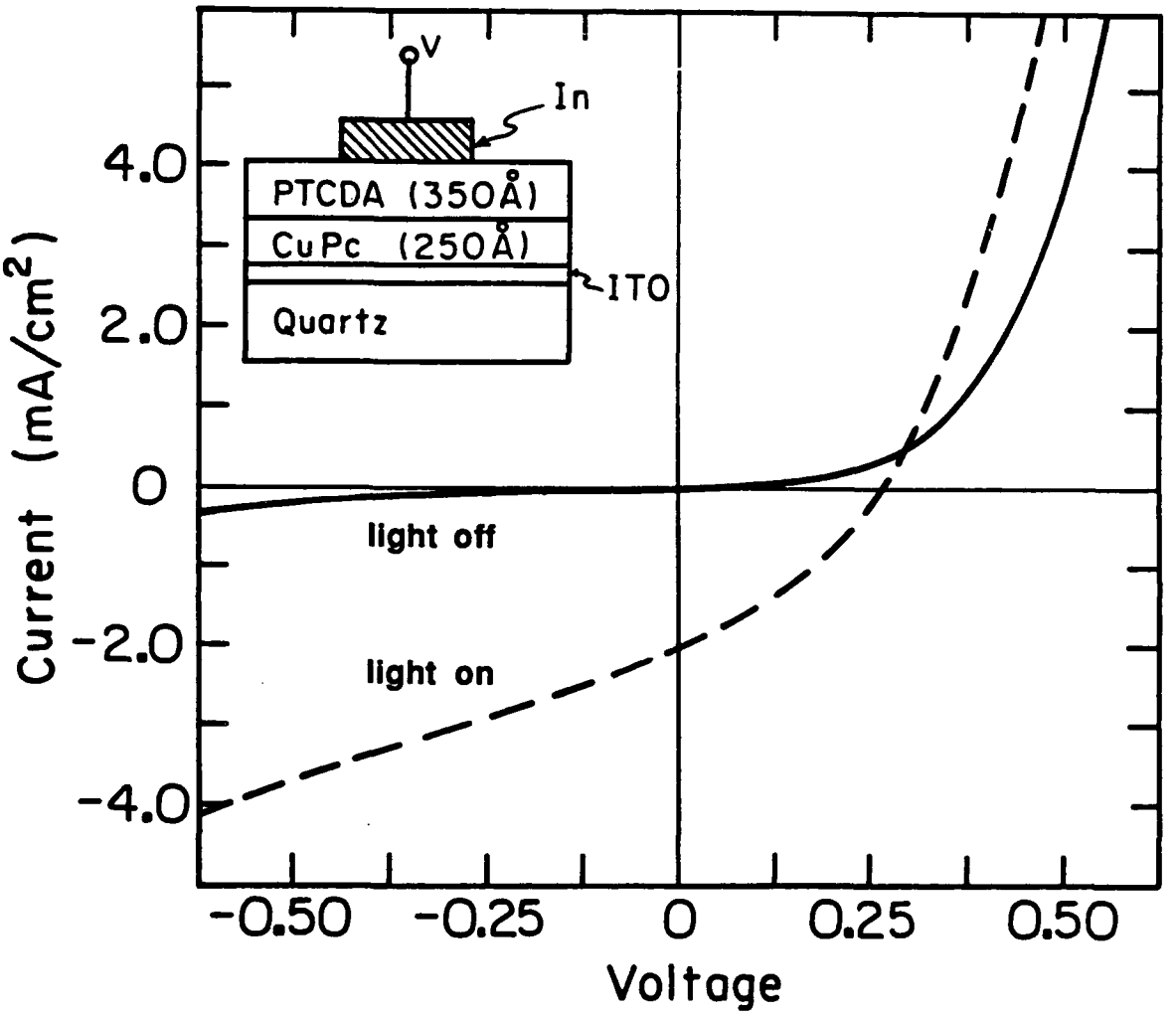
V
In
PTCDA (350Å)
CuPc (250Å)
ITO
Quartz
4.0
2.0
0
-2.0
-4.0
Current (mA/cm²)
light off
light on
-0.50
-0.25
0
0.25
0.50
Voltage

FIGURE 1

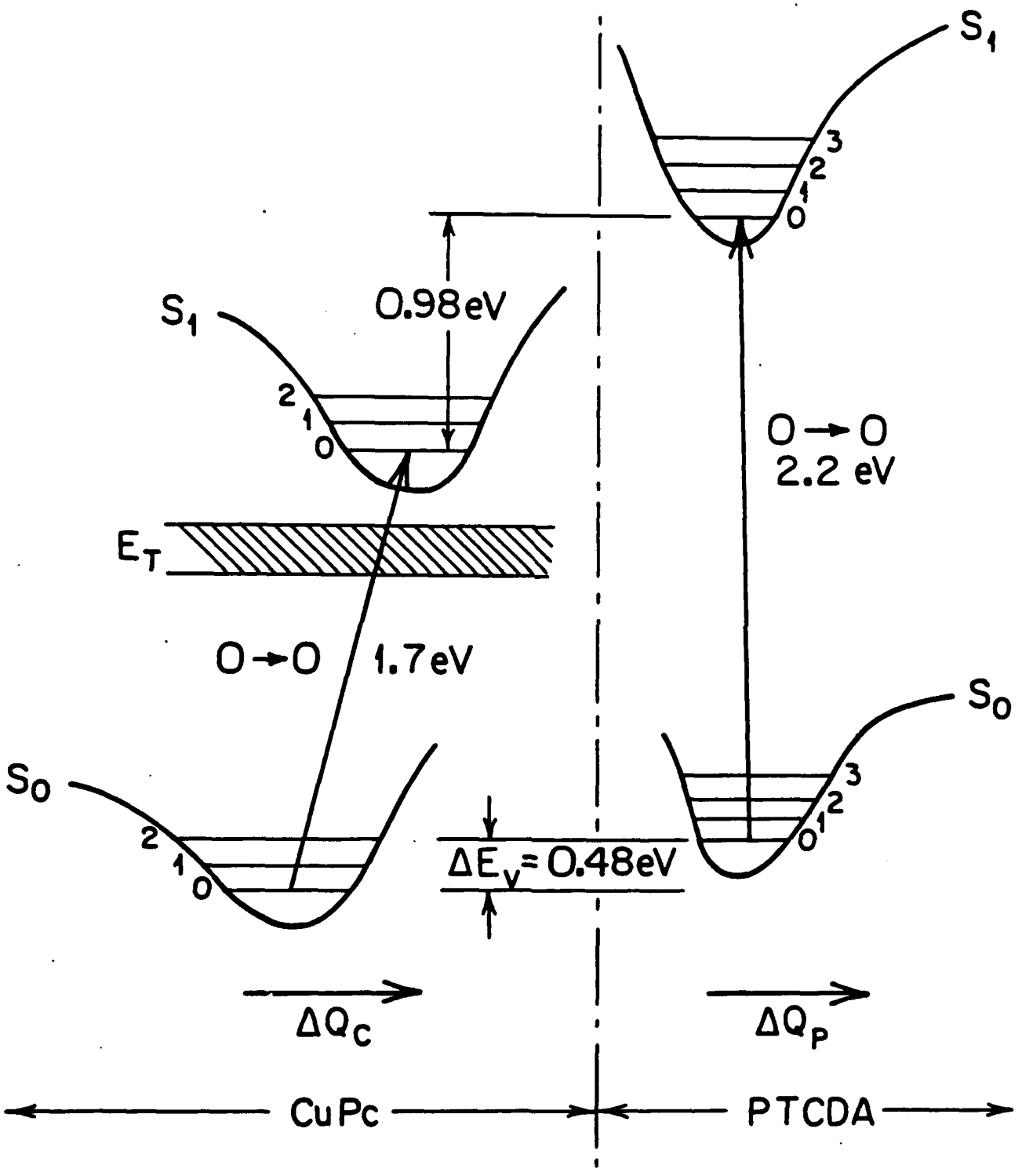
S1
3
2
1
0
0.98eV
S1
2
1
0
O→O
2.2 eV
ET
O→O 1.7eV
S0
2
1
0
S0
3
2
1
0
ΔEV=0.48eV
ΔQC
ΔQP
CuPc
PTCDA

FIGURE 2

As a result of the good electrical properties of these heterojunctions which are largely trap free, and due to the ability to grow crystalline HJ's without requiring lattice match between the contacting semiconductors, we regard this work as indicative of the enormous potential of crystalline organic semiconductors to serve in a wide range of optoelectronic device applications.

Publications

1. S. R. Forrest, L. Y. Leu, F. F. So, and W. Y. Yoon, "Optical and Electrical Properties of Isotype Crystalline Molecular Organic Heterojunctions," J. Appl. Phys., **66**, 5908 (1989).

2. F. F. So, W. Y. Yoon, L. Y. Leu, and S. R. Forrest, "Growth and Characterization of Organic Semiconductor Heterojunctions and Quantum Well Structures," SPIE Symposium on the Growth of Semiconductor Structures and High T_C Films on Semiconductors, San Diego (March 1990).

Research to Improve Long Wavelength Infrared Semiconductor Opto-Electronic Devices

Elsa Garmire

Research Unit QE2-1

Progress

This project is to look for ways of improving long wavelength semiconductor opto-electronic devices. The effort is motivated by the need to reduce the effects of nonradiative Auger recombination. The approach is to use similar concepts for semiconductor laser development and nonlinear optical devices. Motivated by the results of experiments in GaInAsP at 1.06 μm, we are exploring how n-i-p-i structures may be used to separate charges, lengthening carrier lifetimes and reducing Auger recombination. The research activities during this year have been focused on two areas. First, liquid phase epitaxy of InAsPSb of reasonable quality and repeatability has been achieved after InAs buffer layer growth. Second, computer simulation of InAs/InAsPSb double heterostructures has been carried out to find out the distributions and lifetimes of carriers in structures with properties strongly affected by carrier transport, such as n-i-p-i structures.

Material Growth and Characterization. InAsPSb liquid phase epitaxial layers grown by the step cooling technique had been shown to have less compositional variation along the growth direction than those grown by equilibrium cooling technique. Therefore, the first change we made was to have a single phase melt which ensures supersaturation below the saturation temperature. A recipe was predicted based on thermodynamic calculations. However, the saturation temperature of the melt is very sensitive to the P content and is difficult to experimentally determine. In order to achieve reproducibility, we employed the source dissolution technique which allowed us to have much better control over the saturation temperature and composition of the melt. It also helped to modify predictions from thermodynamics for growing layers with slightly different compositions. Typical lattice mismatch we have achieved is abut 0.05% and the carrier concentration of an n-type undoped layer is about $10^{17}/cm^3$. Progress is underway to dope and make PnP structures.

Simulation Result and Prediction. Continuing from the concept of selective confinement of carriers developed last year, we simulated device structures in order to determine the confinement of both carrier types. Simulation was done with PUPHS (Purdue University Program for Heterostructure Simulation) which solves Poisson's equation and continuity equations for electrons and holes. Structures which have been simulated are of two types. One is a layer of narrow-bandgap i-InAs of thickness d_n sandwiched between two layers of wider-bandgap P-InAsPSb. This is a hetero-PnP structure. The other replaces the single n-InAs layer in the above structure with an nPn InAs/InAsPSb/InAs superlattice. Carriers are generated in InAs by absorption of incident light. The doping level we chose for the n-type layers is $1.5 \times 10^{18}/cm^3$ and $10^{18}/cm^3$ for p-type layers. The actual bang lineup for this heterostructure is not exactly known, but believed to be a staggered lineup. This means that the valence band of InAs lies below that of InAsPSb, an assumption we used in our analysis.

We simulated optical pumping to describe nonlinear optical devices and optically pumped lasers. As the incident light intensity increases, the minority carrier density in each layer increases as well. The distribution of these excess carriers results from diffusion-drift and recombination-generation processes. Due to accumulation of free charges the valence bands of InAs and InAsPSb come to the same energy level except for small regions near the heterointerfaces. Further increase of the incident light intensity will move the valence band of InAs higher and holes will begin to accumulate in the InAs layer. Keeping in mind that we want to have p=fn where f is the ratio of coefficients of Auger processes due to electrons and holes (estimated to be smaller than 0.3), we ended the simulation under this flat valence band condition. The current density generated under this condition is around 20 to 30 kA/cm^2.

We found that the ratio of the concentrations of electrons and holes decreases with increasing incident light intensity. When the valence bands of the two materials coincide, this ratio is about 0.92. When the ratio was 0.3 as desired,t he concentrations were too low to give a positive gain; the gain calculated from band-to-band radiative recombination was negative. As a result, our task has been to find a structure with proper dimensions that will discriminate the two carriers more strongly.

We noticed that electrons accumulate near the heterointerfaces in InAs but the holes are depleted, so that the ratio of the two is much higher at the interfaces than that in the center of the active region. Also, at the interface, the concentrations are large enough to achieve positive gain. However, the gain is small compared with that outside the InAs accumulation region. Thus, it is important to reduce the thickness of the InAs layer to less than 1000Å. This indicates the need for a hetero-nipi superlattice as the active region. We have modelled the hetero-nipi using PUPHS with 1000Å layers and we are now working on understanding how to average this model over the optical mode volume.

Publications

1. N. M. Jokerst, "Nonlinear Optical Absorption in Single Heterostructure Schottky Barrier Epitaxial Structures," USC Ph.D. Thesis (May 1989).

2. E. Garmire, N. M. Jokerst, A. Kost, A. Dap[illegible], and P. D. Dapkus, "Optical Nonlinearities due to Carrier Transport in Semiconductors," JOSA B, **6**, 579 (1989).

3. N. M. Jokerst and E. Garmire, "Nonlinear Optical Absorption in Semiconductor Epitaxial Depletion Regions," Appl. Phys. Lett., **53**, 897 (1988).

4. N. M. Jokerst, and E. Garmire, "Nonlinear Absorption in Semiconductor Single Heterostructure Schottky Barrier Structures," QELS '89, Paper MBB2 (1989).

5. N. M. Jokerst and E. Garmire, "Modelling of Nonlinear Absorption in Semiconductor Single Heterostructure Schottky Barrier Devices," OSA Annual Meeting, Paper ML1 (1989).

A Spectroscopic Study of Basic Processes in Electrically Excited Materials

M. Gundersen

Research Unit QE2-2

Progress

Avalanche breakdown in p-n AlGaAs/GaAs heterojunctions was investigated, and the maximum electric field, the breakdown voltage, and the depletion-layer width are calculated as functions of the AlAs composition in AlGaAs and of the doping densities on both sides of the junction. The model employed is an extension of Hauser's model of homojunction breakdown.

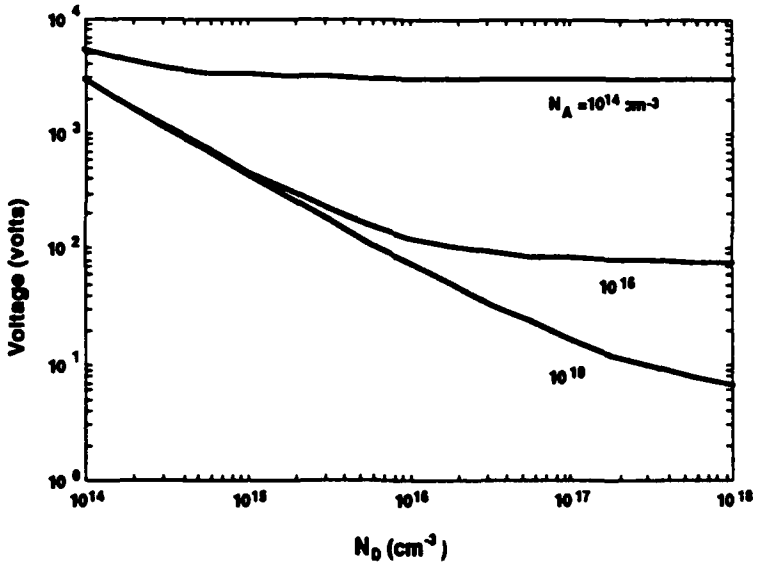

FIGURE 1. Avalanche Breakdown Voltage of p-n AlGaAs/GaAs Heterojunctions as a Function of Donor Concentration (N_A). The AlAs Composition x in AlGaAs is 0.3.

An optically gated, GaAs bipolar junction thyristor with a semi-insulating base layer, specifically developed for pulsed power applications, has been fabricated and tested. The measured DC blocking voltage of the device was >600 volts, peak pulsed current was >70 A, and the current rise rate was $1.4 \cdot 10^9$ A/sec. These results demonstrate that GaAs based junction devices have significant potential as switching elements for pulsed power systems requiring very fast closing times.

Theoretical considerations and fabrication principles for the design and development of GaAs based "Static Induction" transistors and thyristors for pulsed power applications are presented. Compared to silicon SITs, lower on-resistance and faster switching speeds are expected. Devices are being fabricated based on implementation of chemically etched "recessed-gate" Schottky structures for improved blocking voltage capability.

A thyristor-like optoelectronic switch with high current density, based in GaP, was investigated. The switch is based on the optoelectronic bistability exhibited by certain GaP light emitting diode-type structures at 77K. The bistability is based on the negative differential resistance that occurs during the forward biased current-voltage (I-V) characteristics. A model has been developed to explain the observed s-shape I-V characteristic and describe the dependence of the I-V characteristic on the geometry of the device, doping species and concentrations. The switching time depends on the intensity of optical gating signal, bias voltage and doping concentrations. The device has high current density capability (~10^4 A/cm^2), can be triggered optically, and its geometry and doping concentrations can be readily controlled and varied. The model has a general applicability to III-V based pulsed power switches.

Publications

1. H. H. Dai, M. S. Choi, M. A. Gundersen, H. C. Lee, P. D. Dapkus, and C. W. Myles, "Phonon-Assisted Recombination in GaAs/AlGaAs Multiple-Quantum-Well Structures," J. App. Phys. 66 (6), 2538 (1989).

2. J. H. Hur, C. W. Myles, and M. A. Gundersen, "Avalanche Breakdown in p-n AlGaAs/GaAs Heterojunctions," submitted to J. Appl. Phys.

3. P. Hadizad, J. H. Hur, M. A. Gundersen, and H. R. Fetterman, "Design of an Opening and Closing GaAs Static Induction Transistor for Pulsed Power Applications," Proceedings, Seventh IEEE Pulsed Power Conference, Monterey, California (June 1989).

4. J. H. Hur, P. Hadizad, M. A. Gundersen, and H. R. Fetterman, "A GaAs-AlGaAs Based Thyristor," Proceedings, Seventh IEEE Pulsed Power Conference, Monterey, California (June 1989).

5. C. W. Myles, J. H. Hur, and M. A. Gundersen, "Avalanche Breakdown in p-n AlGaAs/GaAs Heterojunctions," Proceedings, Seventh IEEE Pulsed Power Conference, Monterey, California (June 1989).

6. S. D. Tsiapalas, J. H. Hur, M. S. Choi, and M. A. Gundersen, "A High Current Density Thyristor-Like Gallium Phosphide Based Optoelectronic Switch," Proceedings, Seventh IEEE Pulsed Power Conference, Monterey, California (June 1989).

7. "The back-lighted thyratron", in "Optics in 1989", Optics News **15**, 37 (1989), (invited).

8. J. H. Hur, P. Hadizad, S. G. Hummel, D. M. Dzurko, P. D. Dapkus, M. A. Gundersen, and H. R. Fetterman, "GaAs Based Opto-Thyristor for Pulsed Power Applications," Proceedings, IEDM (1989).

9. M. Choi, "A Study of Optical Device Based in Gallium Phosphide," Ph.D. Thesis (December 1989).

Nonlinear Optical Waveguiding in Compound Semiconductors

William H. Steier

Research Unit QE2-3

Progress

The objective of this unit is twofold:

1. To make measurements of the linear and nonlinear optical properties of multiple quantum well structures using waveguiding techniques, and

2. to invent, analyze, and demonstrate some novel new nonlinear optical devices based on a waveguiding structure. In both of these areas, we have made progress.

Measurement of the absorption coefficient of MQW materials in the low loss region, approximately 50meV from the band edge, are important for several reasons. They provide information on the physical nature of the exciton resonance and the band edge, they give some insight into the material and interface quality, and, perhaps most important they provide device design data on the optimum wavelength range for device operation. In general, the optimum wavelength for operation of nonlinear optical devices such as optical switches and bistable devices is the region where the ratio $\Delta n/\alpha$ is the largest. In this ratio, Δn is the magnitude of the nonlinear change in the index of refraction and α is the absorption coefficient.

Waveguiding techniques for MQW loss measurement are a powerful approach because a wide wavelength range and a wide range of absorption coefficients can be measured in a single material. One can vary the interaction length over a wide range, vary the guide filling factor widely by placing the MQWs either in the waveguide or in the cladding, and vary the number of quantum wells. The waveguide etalon finesse measurements enable one to get an absolute loss measurement independent of the coupling loss. In addition both TE and TM polarizations are available.

Absorption Coefficient Measurements

To demonstrate the strength of the method we have made a series of loss measurements on AlGaAs/GaAs MQWs from the exciton peak out to greater than 40meV on the long wavelength side where the absorption coefficient varies by two orders of magnitude. The waveguide structure, shown in Fig. 1, has the quantum wells in the cladding and uses an etched 1μm ridge for lateral confinement. By using several cleaved lengths of waveguide ranging from 0.49mm to 8.2mm we were able to measure the absorption coefficient over the range shown in Fig. 2. The absorption coefficients are the actual waveguide loss and to be converted to the MQW material loss they must be multiplied by 55 to account for the guide filling factor.

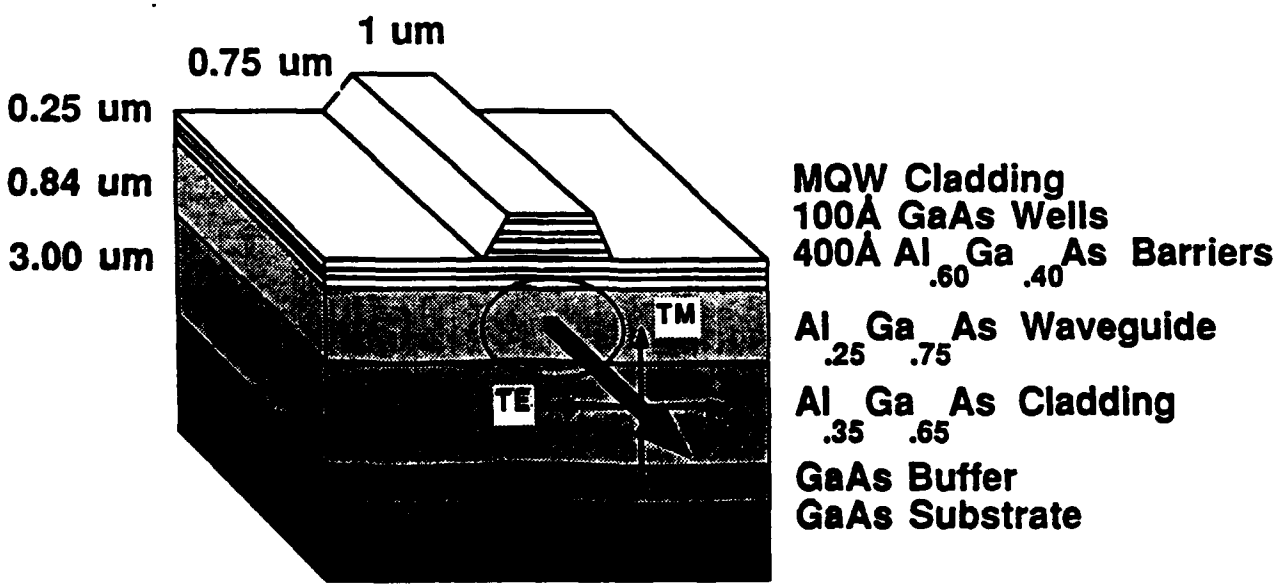

Power Filling Factor 1.8%

FIGURE 1. MQW Waveguides

TM Absorption Spectrum

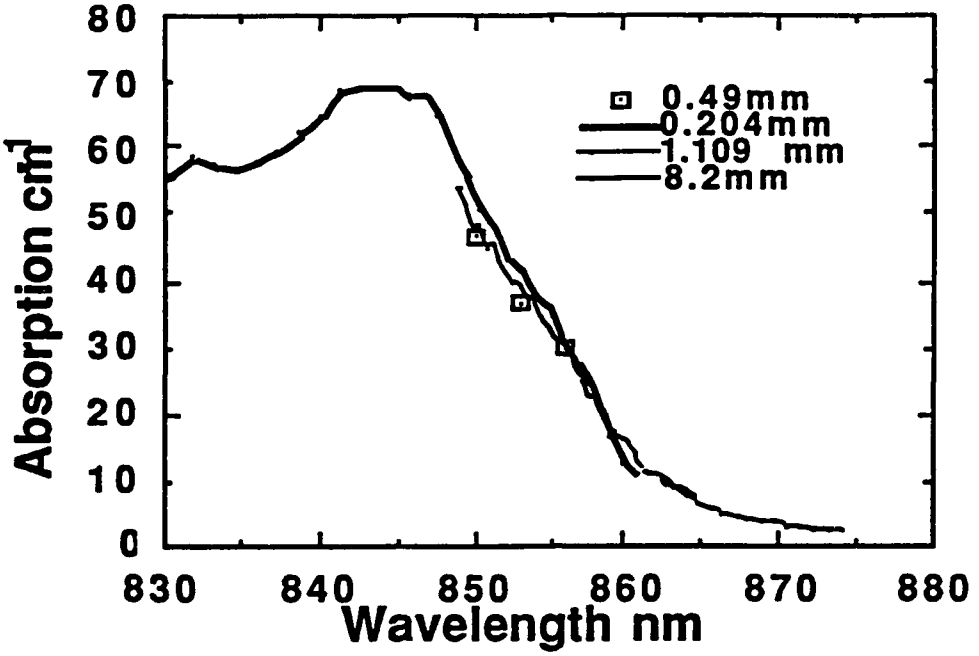

TE Absorption Spectrum

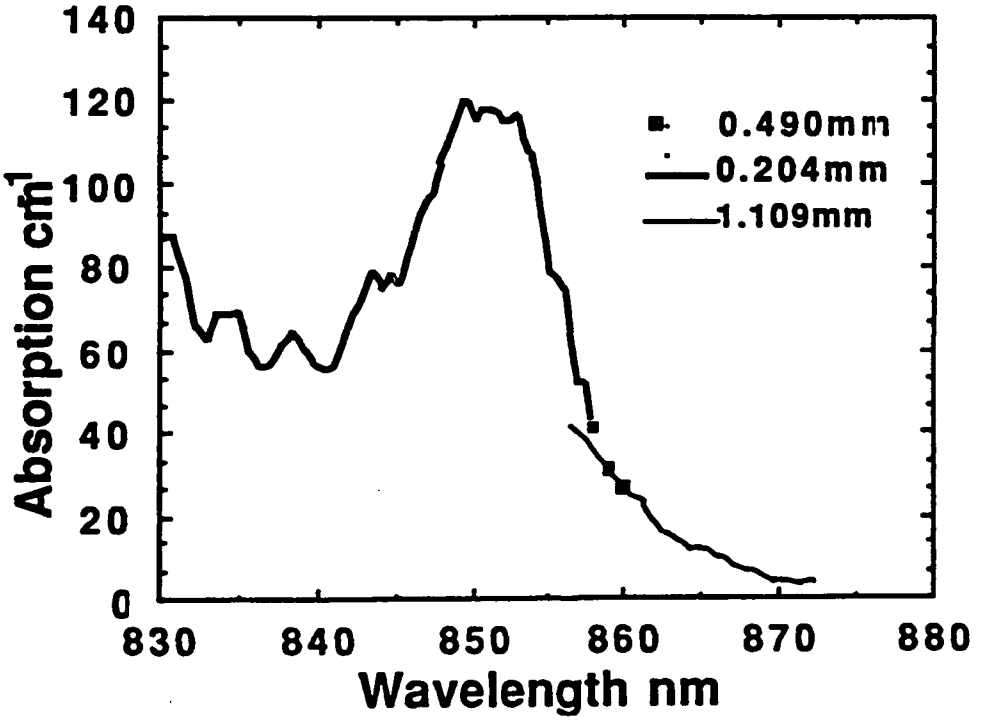

FIGURE 2. MQW Absorption Spectra

To calibrate the guide coupling loss, the etalon finesse technique was used for waveguide lengths and in the wavelengtn range where the guide loss was in the 10 to 40cm^{-1} range. In this loss range the cleaved waveguides make a sufficiently high finesse etalon for measurement of the finesse as the wavelength is tuned. From the known specular reflection of the cleaved ends and the measured finesse, the waveguide loss coefficient can be calculated. These measurements enabled us to account for the coupling loss in the transmission measurements since the measurements for the various lengths overlapped the wavelength range where the etalon technique was used. The waveguide scattering loss was accounted for by measuring the guide loss at 1.5μm where the MQW loss is negligible.

These loss measurements were made with a computer controlled dye laser and automated data collection system. The laser source was pulsed at 150nsec to prevent heating and the transmission measurement at each wavelength was the average of several pulses taken by a boxcar integrator to improve the signal to noise. All measurements were made at a sufficiently low intensity to avoid any saturation of the loss.

From these measurements the Urbach parameter of the MQW material, E_o, was determined. The Urbach parameter describes the tail of the band edge or the exciton resonance by

$$\alpha = \alpha_o \exp(\Delta E/E_o)$$

where α_o is the peak absorption and ΔE is the distance from the peak. The measured Urbach parameters for the TE and the TM polarization are:

$$E_{oTE} = 7.7\text{meV}$$
$$E_{oTM} = 9.5\text{meV}.$$

The difference between the Urbach parameters for the two polarizations gives direct confirmation that the Urbach absorption is band dependent. The difference is consistent with potential well models which take into account the difference in the heavy and light hole masses for the bands excited by the TE and TM polarization. MQW theory (John, 1988) shows that the ratio of the TE and TM Urbach parameters

should be inversely proportional to the ratio of the reduced masses of the heavy and light holes.

$$E_oTE/E_oTM = m^*lh/m^*hh$$

Our measurements give this ratio of the masses to be 0.81 which is in reasonable agreement with effective mass data which has been published (Miller, 1987) which gives this ratio as 0.70.

Typical Urbach parameters for bulk GaAs vary from 7.0 to 7.8. Since our quantum well material showed similar Urbach parameters, the MOCVD grown MQW material is shown to be of high quality with low impurity levels.

The different spectra of the absorption coefficient for the TE and TM polarizations due to the different contributions of the heavy and light hole excitons make any waveguide device which contains quantum wells exhibit dichroic loss which is wavelength dependent. However because of the different Urbach parameters there is a wavelength where the loss of the TM and TE polarizations is the same. This wavelength is of potential interest for devices since the dichroism is zero. Our measurements do not extend to a long enough wavelength to observe the zero dichroism but from the measured Urbach parameters this wavelength can be calculated. The calculated zero dichroism wavelength for the 100A wells is 886nm.

A High Contrast, Low Switching Energy Optical Switch

We have completed an analysis of an optical switch using waveguiding in MQW material which predicts a high on/off contrast ratio and low required switching energy. High contrast switches are desirable in multilayer switching fabrics where considerable fan-in and fan-out is necessary. In these switch matrices, the output of one switch is used to control several other switches and a high contrast ratio makes it possible for the next layer to distinguish a stimulating signal from noise. All bistable devices and directional coupler devices which rely on output intensity changes have on/off contrast ratios limited to 3:1 or less (Gibbs, 198- and Wa, 198-). The device we have analyzed makes use of the saturable *birefringence* in MQW waveguides to give a predicted contrast ratio of 9000:1.

The required switching energy can be greatly reduced by making use of the larger $C^{(2)}$ effects coupled with charge separation. In MQWs the $C^{(2)}$ effects include the quantum confined Stark effect, the Franz-Keldysh effect, and the electrooptic effect. The charge separation occurs when the MQWs are placed in the intrinsic region of a back biased pin diode. Using this approach the required switching intensity can be reduced by about eight orders of magnitude. The price one pays for this improvement is a slower switching speed which is now limited by the circuit RC time constant. Typical RC time constants are 10nsec in the devices we have analyzed.

In cooperation with the Compound Semiconductor Laboratory under Prof. P. D. Dapkus, we are now proceeding to fabricate a prototype switching device.

Publication

1. W. H. Steier and R. T. Sahara, "Direct Measurement of Urbach Absorption in AlGaAs/GaAs Quantum Well Waveguides," Paper OE 2.2, 1989 LEOS Annual Meeting, Orlando, FL (October 1989).

Parallel Optical Processing in Photorefractive Materials

Jack Feinberg

Research Unit QE2-4

Progress

We have been studying the photorefractive effect in barium titanate crystals. Although the usual theories predict that the photorefractive speed in these crystals should increase linearly with the optical intensity I, we previously found that in all as-grown crystals the photorefractive speed scaled sublinearly, namely as I^x, with the exponent ranging from x=0.5 to x=0.9 depending on the particular sample. This sublinear intensity scaling law has practical importance: it implies that high-speed operation of a photorefractive device will require more light energy than previously suspected.

In this past year, we solved the puzzle of the apparent sublinear dependence of photorefractive speed on intensity in $BaTiO_3$, and we show that the culprit is a level of shallow acceptors. The nonlinear scaling of photorefractive speed with intensity is caused by the change in the number of empty sites in the deep levels due to partial filling of the shallow level. If the shallow level were to remain either completely empty or completely full, then the crystal's speed with increase linearly with intensity.

We identify two types of barium titanate crystals which we call type *A* and type *B*. A type *A* crystal has an erasure speed that increases almost linearly with light intensity (speed $\alpha\, I^{x=0.9}$), a steady-state photorefractive grating strength that varies very little with intensity, and a small dark conductivity. A type *B* crystal has an erasure speed that increases decidedly less-than-linearly with light intensity, (speed $\alpha\, I^{x=0.6}$), a steady-state photorefractive grating strength with a marked intensity dependence, and a large dark conductivity. We show that a simple two-level model of deep donors and shallow acceptors explains the very different behaviors of these two types of $BaTiO_3$ crystals.

We postulate that in type A crystals the number density of donors exceeds that of acceptors ($N_D >> N_A$), while in type B crystals the two number densities are comparable ($N_D \leq N_A$). We consider the case where charges in *both* the donor and the acceptor levels can be excited by light. For simplicity, we consider transport only by holes. We position the donor impurities with density N_D near the middle of the band gap of the crystal (which is ~ 3.1 eV for $BaTiO_3$) and the acceptors with density N_A close to the top of the valence band, so that at room temperature holes can be thermally excited from the acceptor level (but not from the donor level) into the valence band. Experimentally we find that the shallow acceptor level is located 0.4 eV from the valence band. The Fermi level is located on the donor levels for $N_D > N_A$ and on the acceptor level for $N_D < N_A$. By solving the coupled differential equations governing the transport of charges between the two levels and the valence band, we obtain theoretical curves that show a nonlinear scaling of speed on light intensity.

An important result of our theory is that the function I^x is not, in fact, the correct functional dependence of the photorefractive speed on light intensity; the actual function is considerably more complicated. However, when plotted on a log-log graph the correct function mimics an I^x dependence. We found that it is more instructive to plot not the speed but the total energy density Φ needed to erase a photorefractive grating, as shown in Fig. 1. Horizontal regions of this curve correspond to a linear dependence of speed on intensity. It is seen that both type A and B crystals have both linear and sublinear regions of intensity dependence.

We performed detailed experiments to confirm our theory. We measured the light-induced erasure rate of photorefractive gratings uin $BaTiO_3$ crystals as a function of the incident light intensity.

Fig. 2 is the plot of Φ vs. I_0 in the Rob crystal (a type A crystal) for three temperatures. Note that at low intensity the curve is quite flat, so this crystal's speed will scale linearly with intensity in this region. Fig. 3 shows a plot of Φ vs. I_0 for the Cat crystal, a type B crystal. Now the function Φ is seen to increase with light intensity even at low intensities, which implies that the density of the ionized donors is changing appreciably even at low intensities. At high intensity Φ is seen to flatten, because the density of holes in the shallow acceptors (and the corresponding

density of ionized donors) is beginning to saturate. Note that the data corresponding to higher crystal temperatures flatten at higher intensities, because an acceptor level with an increased thermal excitation rate requires more light to fill it.

Publications

1. Jack Feinberg and Kenneth R. MacDonald, "Phase Conjugate Mirrors and Resonators with Photorefractive Materials," Chapter 5 in Topics in Applied Physics, **62**: Photorefractive Materials and Their Applications II, Springer-Verlag (1989).

2. D. Mahgerefteh and J. Feinberg, "Explanation of the Apparent Sublinear Photoconductivity of Photorefractive Barium Titanate," submitted 12-27-89 to Physical Review Letters.

3. D. Mahgerefteh, "The Speed of the Photorefractive Effect, Shallow Traps, Photogalvanic Currents, and Light-Induced Surface Damage in $BaTiO_3$," Ph.D. Thesis (December 1989).

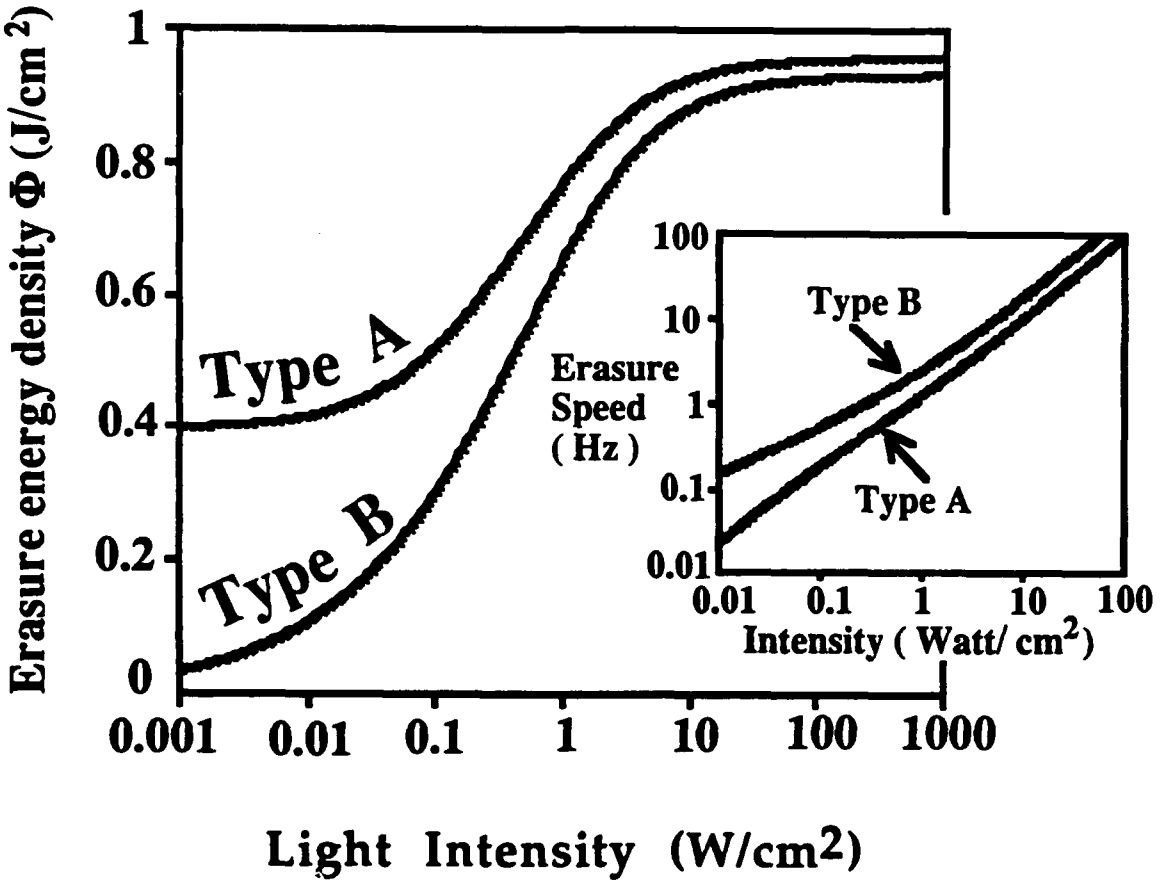

Figure 1. Predicted dependence of Φ (the energy density required to erase a photorefractive grating to 1/e of its initial value) on light intensity for the two types of $BaTiO_3$ crystals. Horizontal regions of this curve correspond to a *linear* dependence of photorefractive speed on intensity. Inset: Log-log plot of the calculated erasure rate vs. intensity showing the apparent I^x behavior.

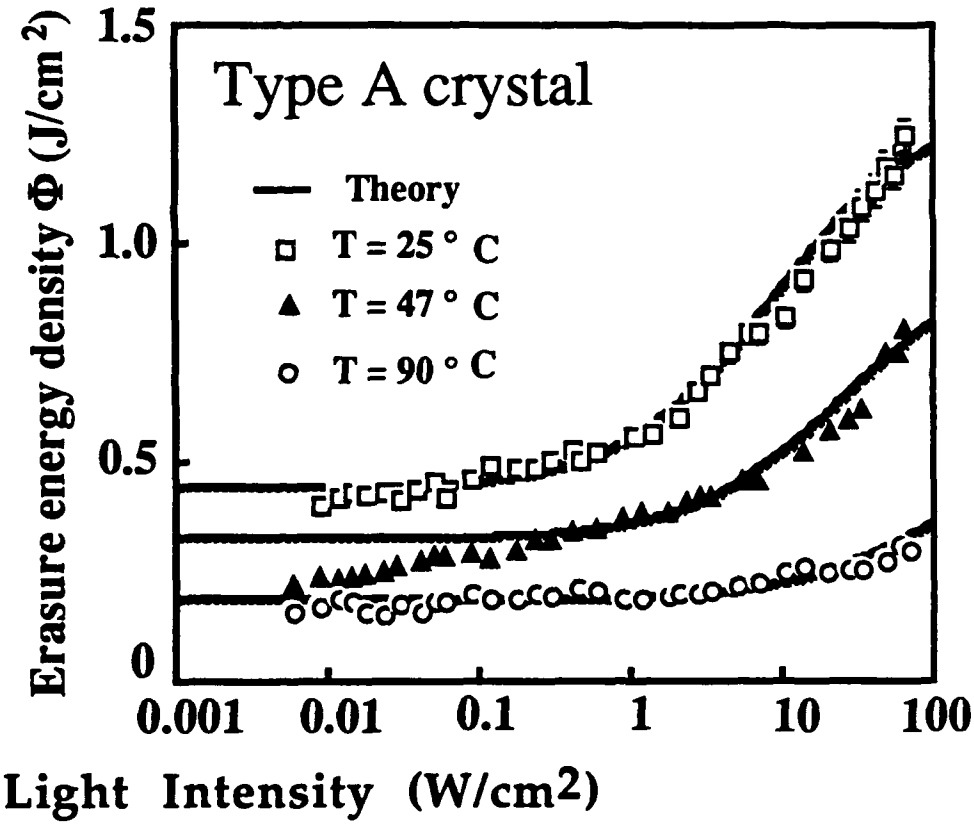

Figure 2. Φ versus I_0 at various temperatures of the Rob crystal of $BaTiO_3$, a type *A* crystal. Solid curves are simultaneous best fits to our two-level theory

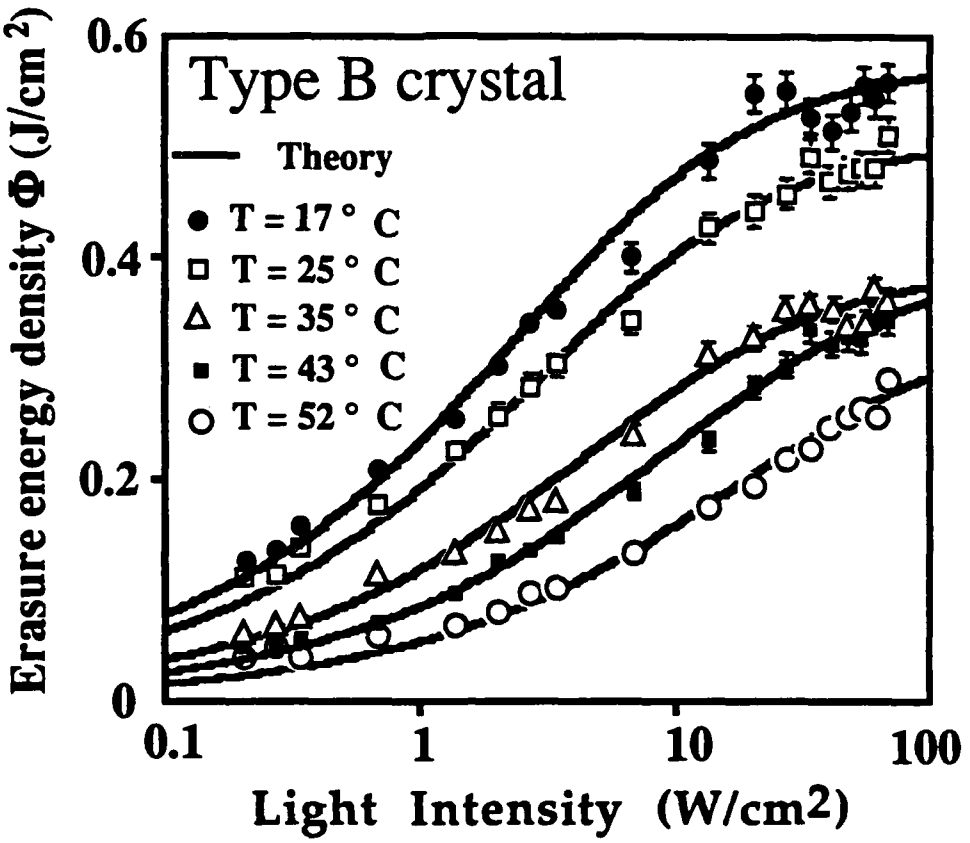

Figure 3. Φ versus I_0 at various temperatures of the Cat crystal of $BaTiO_3$, a type B crystal. Solid curves are best fits to our theory

Spread Spectrum Receiver Design for Intense Jamming Environments

R. A. Scholtz

Research Unit IE2-1

Progress

In this research on communications in intense jamming environments, we are attempting to quantify the performance of a spread-spectrum receiver consisting of an analog adaptive whitening filter (for pre-despreading interference rejection) followed by a conventional analog code tracking loop. Fig. 1 shows a transform domain realization of the whole system under investigation. (There are several possible implementations of the required processing.)

Since our last report, we have made a slight modification in the first stage of this system, i.e. the transform domain pre-despreading processor now contains a moving window average operating on a raw spectral estimate. The moving average window is chosen to have width between the chip duration and the data bit duration, such that a smoothed spectral estimation with smaller variance and higher reliability is obtained as its output.

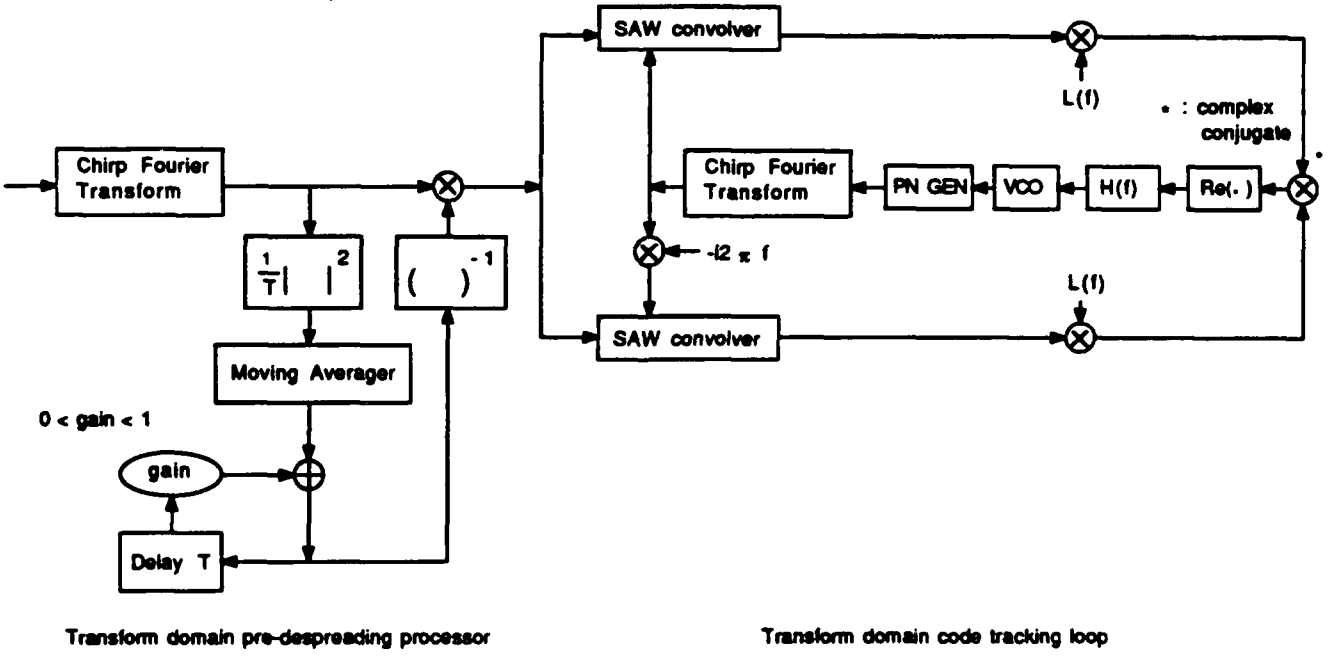

FIGURE 1. Transform Domain Realization of the Whole System

The effectiveness of this pre-despreading processor has been verified by numerical waveform simulations on the Block Oriented System Simulator (BOSS). As a comparative test, two systems, one with the pre-despreading processor shown in Fig. 1, and the other without, were operated on the same DS/SS-BPSK signal, along with white Gaussian noise and randomly switched (on/off) tone jammer located on the carrier frequency. The results of these simulations indicate that (a) the bit error probability is reduced dramatically when the pre-despreading whitening filter is in place, and (b) the effectiveness of this processor diminishes gradually as the average on/off period decreases (i.e., the interference becomes white).

Although the simulation seems to be fairly easy with the aid of BOSS, the analysis of the *precise* statistical properties of the output of the whitening filter have proved to be difficult. To study the performance of the code tracking loop, we must at least crudely estimate the statistical characteristics of the incoming waveform at the front end of the tracking loop. It is clear that this waveform can be viewed as the ratio of two processes, with the numerator being a linear operation on the receiver input. However, the denominator is difficult to analyze since it is the result of a combination of linear and nonlinear operations on the receiver input.

Recently, we switched our research focus from trying to find the precise statistical properties of the adaptive whitening filter output, to trying to get better insight into how the time-varying S-curves and effective noise power densities of the equivalent tracking loop are related to parameters of the jamming process. We have begun this phase by making a naive assumption that the adaptive whitening filter can respond to the non-stationary jamming instantaneously. After developing a basic understanding of the tracking loop's response to jamming in this simplified environment, we hope to incorporate more realistic assumptions about the statistical characterization of the effects of the whitening filter.

Basic Research in C^3 Distributed Databases

Victor O.K. Li

Research Unit IE2-2

Progress

In the past year, we have focused on three areas of basic research in distributed databases, namely, concurrency control algorithms, query processing, and failure recovery protocols. The Unified Model for Concurrency Control Algorithm, described in Pub. 6, provides a framework with which one can study and evaluate the performance of different concurrency control algorithms. In Pub. 1, a performance model has been developed for locking algorithms which incorporates the effect of deadlocks. We found that the traditional approach of resolving deadlocks by aborting some transactions is extremely costly. Therefore, we have developed a new abortion-free deadlock detection-resolution algorithm (Pub. 7). In the area of Query processing, we have developed the domain-specific semijoin for distributed query processing (Pub. 2), and a query processing algorithm applicable to distributed databases managed on local area networks (Pub. 3). We have also developed termination protocols in distributed databases managed on networks with unreliable components (Pubs. 4 and 5).

Publications

1. S. C. Shyu and V.O.K. Li, "Performance Analysis of Static Locking in Distributed Database Systems," to appear in the IEEE Trans. on Computers.

2. J.S.J. Chen and V.O.K. Li, "Domain-Specific Semijoin: A New Operation for Distributed Query Processing," to appear in Information Sciences.

3. J.S.J. Chen and V.O.K. Li, "Optimizing Joins in Fragmented Database Systems on a Broadcast Local Area Network," IEEE Trans. on Software Engineering, **SE-15**, No. 1, 26 (January 1989).

4. C. L. Huang and V.O.K. Li, "Missing-Partition Dynamic Voting Scheme for Replicated Database Systems," Proc. IEEE International Conference on Distributed Computing Systems, 579, Newport Beach, CA (June 1989).

5. C. L. Huang and V.O.K. Li, "A Quorum-Based Commit Protocol and its Termination Protocol for Distributed Database Systems," submitted for publication.

6. C. P. Wang, and V.O.K. Li, "A Unified Model for Distributed Database Concurrency Control Algorithms," submitted for publication.

7. S. C. Shyu and V.O.K. Li, "An Abortion-Free Distributed Deadlock Detection-Resolution Algorithm for Distributed Database Systems," submitted for publication.

SEGMENTATION AND 2-D MOTION ESTIMATION OF NOISY IMAGE SEQUENCES

Alexander A. Sawchuk **Research Unit IE2-3**

Progress

In previous work we have combined two important problems in scene analysis of image sequences: the segmentation of image frames into moving and non-moving components; and the 2-D motion estimation of the moving parts of the scene. These parts are interactively connected in a mutually beneficial way.

Our work during this reporting period has concentrated on the extension of these results to noise suppression and enhancement of a very noisy sequence of images of a moving object. There are two steps to the algorithm. First, a combined segmentation and motion estimation algorithm is employed. Then a temporal or a spatiotemporal low-pass filter is applied. We have used mean and median filters as low-pass filters. The temporal filtering is performed over the motion path of each pixel, which is provided by the motion estimation algorithm. The spatial filtering does not blur the boundaries of the moving objects because the boundary locations are provided by the segmentation algorithm. The performance of the combined algorithm is examined using computer generated and real image sequences corrupted by additive white gaussian noise.

The time sampling of a time-varying scene produces a sequence of 2-D images. A very important problem in image sequence processing is noise suppression and image enhancement. Although the enhancement of single images has been extensively studied, there has been only a limited study of image sequence enhancement. The intensity of the pixels is spatially and temporally correlated, and the temporal correlation is usually stronger. A temporal low-pass filter can be used to suppress the noise. This filter reduces the variance of the noise but also blurs the moving parts of the scene. Although a temporal low-pass filter is usually the best candidate, because of memory constraints, a spatiotemporal filter is sometimes more desirable. Such a filter will also generally cause degradation by blurring the edges.

The algorithm previously developed under this program segments the images into moving and stationary components and estimates the motion of the moving parts. Then a temporal low-pass filter is applied. For a stationary pixel the filtering is performed over a set of pixels with the same space coordinates. For a moving pixel the filtering is performed over its motion path, which is provided by the motion estimation part, so that the moving parts are not blurred. We have used mean and median filters as low-pass filters and examined the performance of mean filters for different SNR (Signal-to-Noise Ratio) and different kinds of motion. Mean filtering is more effective in the case of white gaussian noise and median filtering is more effective in the case of salt-and-pepper noise and burst noise. When using spatiotemporal filters, the spatial filtering is not performed over the boundaries because their positions are provided by the segmentation part, therefore, the edges are not blurred.

Overall, the motion compensated enhancement algorithm performs very well in a very noisy environment. This algorithm can be used for image sequence quality improvement in industrial, commercial and medical applications as well as a preprocessing step for other operations such as recognition and tracking of moving objects.

Publications

1. D. S. Kalivas, "Segmentation and Estimation of Noisy Image Sequences," Ph.D. dissertation, University of Southern California, Los Angeles, CA (December 1989).

2. D. S. Kalivas and A. A. Sawchuk, "Object Boundary Estimation in Noisy Images," submitted to *IEEE Transactions on Pattern Recognition and Machine Intelligence* (June 1989).

3. D. S. Kalivas and A .A. Sawchuk, "A Region Matching Motion Estimation Algorithm," submitted to *Computer Vision, Graphics and Image Processing* (December 1989).

4. D. S. Kalivas and A. A. Sawchuk, "Segmentation and 2-D Motion Estimation of Noisy Image Sequences," to be submitted to *IEEE Transactions on Pattern Recognition and Machine Intelligence* (January 1990).

5. D. S. Kalivas and A. A. Sawchuk, "Object Boundary Estimation in Noisy Images," *Proceedings Conference on Information and Systems Science 1989,* Johns Hopkins University (March 1989).

6. D. S. Kalivas and A .A. Sawchuk, "Motion Compensated Enhancement of Noisy Image Sequences," to be presented at *IEEE 1990 International Conference on Acoustics, Speech and Signal Processing*, Albuquerque, NM (April 1990).

Mathematical Modelling and Control of Complex Systems - Application to Piezoelectrically Coated Large Space Structures

E. Jonckheere

Research Unit IE2-4

Progress

Our problem is modelling complex systems, to be more precise, systems that are too complex to be modelled from such fundamental principles as Maxwell's equations or Lagrangian dynamics, thereby requiring practical experiments to capture the essence of their behavior.

The example that has captured our attention is a flexible plate coated with a piezo film for active distributed control for large space structure applications.

Essentially, we use the "black box" approach. The system is excited at some specific nodes and the response to the excitation is measured at some other nodes. A typical excitation is the harmonic excitation, i.e., the system is excited by a sine wave. Another excitation is more impulsive in nature, i.e., in case the excitation is, say, a Dirac impulse. In either case, the Input/Output data record is observed, and the problem is to derive a model that matches this Input/Output data record. This model, most of the time a transfer matrix, is subsequently used for active control of the structure via, for example, the H-infinity design method.

The experimental Input/Output data record is finitary in nature. Indeed, in case of sine wave excitation, the system can only be robed at finitely many frequencies. But our objective is to come up with a transfer function model of a complex variable taking value in a continuum of frequencies. This fundamental discrepancy between the finitary nature of the set of frequencies at which the system can be probed and the transfer function model with argument taking value in a continuum of frequencies is at the heart of a major difficulty - how to interpolate between the experimental probing frequencies so as to come up with a transfer function model depending on a continuum of frequencies? Besides, this interpolation has to be done in a way that preserves the basic physical property of the system

being identified. For example, in case of the flexible plate, the transfer function between the force actuators and the rate sensors ought to be dissipative or positive real.

An approach we have developed is the case of an impulsive excitation. In that case, some measurements have to be made on the impulse response of the structure. Part of these measurements - the so-called Markov parameters - reflect the transient behavior of the system, while the other measurements - the so-called moments - rather reflect the steady state behavior of the system. The Markov parameters and moments can be recursively taken into consideration for constructing more and more accurate models, matching more and more experimental measurements. In this case the recursion can be implemented very efficiently, because it amounts to the recursive inversion of a Toeplitz matrix, which can be done efficiently using the celebrated Gohberg-Semencul formula. From another perspective, all of these formulas can also be re-interpreted in the coding context, from which it appears that they bear a strange resemblance with the Berlekamp-Massey algorithm.

Applied to a dissipative structure,t he problem of interpolating a finite set of Markov parameters and moments with a positive real transfer matrix directly yields the positive real partial realization problem, an outstanding, still unsolved system theory problem. We have been able to make some progress along the line of positive partial realization from mixed high frequency/low frequency data.

Regarding the harmonic, i.e., sine wave, excitation, we have focused our attention on three specific topics. First, we have developed Fast Hartley Transform, rather than FFT, algorithms. Secondly, we have investigated some issues related to nonuniform spacing of sample points on the unit circle in Fast Hartley and Fourier transforms. Finally, we have looked at the problem of bounding the interpolation error between sample points. The approach we have been using is based on the notion of "width of an analytic function."

Publications

1. E. Jonckheere and C. Ma, "Combined Sequence of Markov Parameters and Moments in Linear systems," IEEE Transactions on Automatic Control, **AC-34**, 379 (March 1989).

2. E. Jonckheere and C. Ma, "Recursive Partial Realization from the Combined Sequence of Markov Parameters and Moments," Linear Algebra and Its Applications: Special Issue on Linear Control and Systems, **122/123/124**, 565 (1989).

3. E. Jonckheere and C. Ma, "A New Hankel Interpretation of the Berlekamp Massey Algorithm," Linear Algebra and Its Applications, **125**, 65 (1989).

4. J. C. Juang and E. Jonckheere, "Data Reduction in the Mixed Sensitivity H-Infinity Design Problem," IEEE Transactions on Automatic Control, **AC-34**, 861 (August 1989).

5. E. Jonckheere and C. Ma, "Modified Cauer Form," Elect. Lett., **24**, 1488 (1988).

6. E. Jonckheere and C. Ma, "Split-Radix Fast Hartley Transform in One and Two Dimensions," IEEE Transactions on Acoustic, Speech and Signal Processing, to appear (1990).

7. R. Li, "Model Reduction and H-Infinity Control Over a Planar Doman," Ph.D. Thesis (December 1989).

Knowledge-Based Interpretation of Aerial Images

Rama Chellappa

Research Unit IE2-5

Progress

The goal of this research project is to develop a general framework for knowledge-based interpretation of a class of aerial images. The central issues are knowledge representation, search and system revisability during construction and extensibility afterwards. In our framework, scene knowledge, which is hierarchical and structured in nature, is concisely represented using frames. Domain problem solving knowledge, which is typically heuristic in form, is declaratively specified through the use of production rules. The issue of search is addressed by a coherent and efficient traversal of the search space with the aid of an Assumption-based Truth Maintenance Systems (ATMS). This search scheme is well suited for aerial image interpretation as alternative paths can be simultaneously explored and competing contexts directly compared. The *inheritance* mechanism of frames together with procedural attachment in the form of *methods* and *active values* permits object-oriented programming which facilitates modifiability and extensibility. System revisability is further assisted by the use of production rules as they are modular pieces of problem solving knowledge that are easily understood and manipulated.

Within this general framework, we are implementing a system with the goal of detecting a class of buildings in aerial images. The process of building detection is carried out in a hierarchical manner. Pairs of line segments are grouped to form *vertices*. Vertices are then grouped to form *edges*. Edges are composed into *edge* rings. Shadow analysis on *closed rings* is used to make roof hypothesis. A surface-based description of a building is generated for each roof hypothesis. All the elements in the hierarchy are represented using frames. The search scheme based on an ATMS is used to deal with ambiguities in this grouping process. We are also addressing the issue of efficient computation of geometric relationships in the presence of noise.

Preliminary results are quite encouraging. Fig. 1 is a typical aerial image of dimension *320 X 320*. A wireframe rendering of the extracted buildings is given in

Fig. 2. In this figure, only the faces visible from the current viewpoint are shown, and no corrections for occlusions have been included. Occlusions are taken cared of in the gray scale rendering in Fig. 3. A ray casting algorithm is used. The original image is used as a texture map to paint the roofs of the buildings. The walls of the buildings are rendered using a lambertian reflectance model. The rest of the image is painted black.

Currently, we are working on refining this system and later extending it to incorporate the detection of other objects (like roads, airplanes, airports, etc.). Potential applications of this research are in target extraction and identification, incremental reconstruction of 3-D scenes and change detection.

FIGURE 1. A Typical Aerial Image

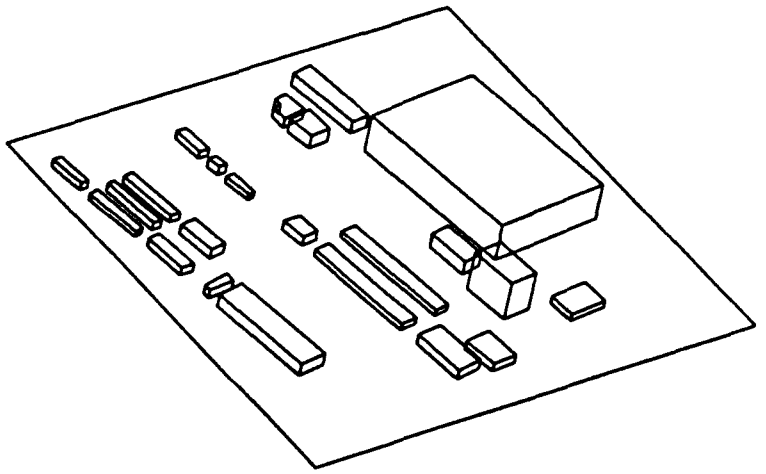

FIGURE 2. The Final Wireframe Interpretation

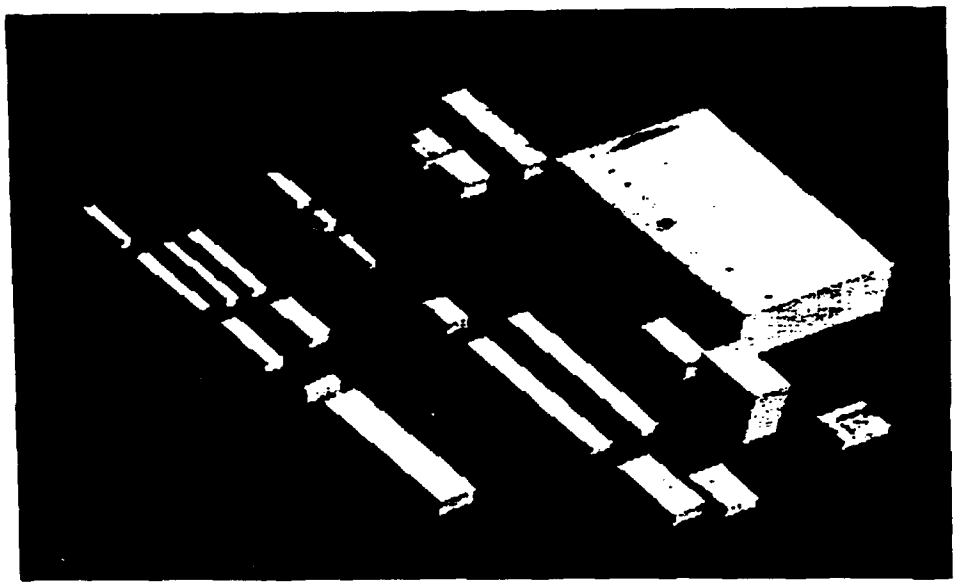

FIGURE 3. Rendering of the Interpretation

Publications

1. V. Venkateswar and R. Chellappa, "A General Framework for the Detection of Buildings in Aerial Images," submitted for publication.

2. Y. T. Zhou, V. Venkateswar, and R. Chellappa, "Edge Detection and Linear Feature Extraction Using a 2-D Random Field Model," IEEE Trans. Patt. Anal. Mach. Intell., **PAMI-11**, 84 (January 1989).

3. A Rangarajan, R. Chellappa, and Y. T. Zhou, "A Model Based Approach for Filtering and Edge Detection in Noisy Images," IEEE Trans. Circuits and Systems (January 1990).

4. R. T. Frankot and R. Chellappa, "Estimation of Surface Topography from SAR Images using Shape from Shading Techniques," Artificial Intelligence Journal (May 1990).

5. A. Rangarajan, R. Chellappa, and T. Simchony, "Deterministic Networks for Image Estimation using a Penalty Function Method," Intl. Joint Conference on Neural Networks, Washington, D.C.